

1 **Underwater CAM photosynthesis elucidated by *Isoetes* genome**

2
3 David Wickell^{1,2}, Li-Yaung Kuo³, Hsiao-Pei Yang², Amra Dhabalia Ashok⁴, Iker Irisarri^{4,5}, Armin
4 Dadras⁴, Sophie de Vries⁴, Jan de Vries^{4,5,6}, Yao-Moan Huang⁷, Zheng Li⁸, Michael S. Barker⁹,
5 Nolan T. Hartwick¹⁰, Todd P. Michael^{10,*}, Fay-Wei Li^{1,2,*}

6
7 ¹Plant Biology Section, School of Integrative Plant Science, Cornell University, Ithaca, NY, USA

8 ²Boyce Thompson Institute, Ithaca, NY, USA

9 ³Institute of Molecular & Cellular Biology, National Tsing Hua University, Hsinchu, Taiwan

10 ⁴Institute for Microbiology and Genetics, Department of Applied Bioinformatics, University of Goettingen,
11 Goettingen, Germany

12 ⁵Campus Institute Data Science, University of Goettingen, Goettingen, Germany

13 ⁶Goettingen Center for Molecular Biosciences, Department of Applied Bioinformatics, University of
14 Goettingen, Goettingen, Germany

15 ⁷Taiwan Forestry Research Institute, Taipei, Taiwan

16 ⁸Department of Integrative Biology, University of Texas at Austin, Austin, TX, USA

17 ⁹Department of Ecology and Evolutionary Biology, University of Arizona, Tucson, AZ, USA

18 ¹⁰The Molecular and Cellular Biology Laboratory, The Salk Institute for Biological Studies, La Jolla, CA,
19 USA

20
21 *Authors of correspondence: T.P.M. (tmichael@salk.edu) and F.-W.L. (fl329@cornell.edu)

22
23 **Abstract:**

24 To conserve water in arid environments, numerous plant lineages have independently
25 evolved Crassulacean Acid Metabolism (CAM). Interestingly, *Isoetes*, an aquatic lycophyte, can
26 also perform CAM as an adaptation to low CO₂ availability underwater. However, little is known
27 about the evolution of CAM in aquatic plants and the lack of genomic data has hindered
28 comparison between aquatic and terrestrial CAM. Here, we investigated the underwater CAM in
29 *Isoetes taiwanensis* by generating a high-quality genome assembly and RNA-seq time course.
30 Despite broad similarities between CAM in *Isoetes* and terrestrial angiosperms, we identified
31 several key differences. Notably, for carboxylation of PEP, *Isoetes* recruited the lesser-known
32 “bacterial-type” PEPC, along with the “plant-type” exclusively used in other terrestrial CAM and
33 C4 plants. Furthermore, we found that circadian control of key CAM pathway genes has
34 diverged considerably in *Isoetes* relative to flowering plants. This suggests the existence of
35 more evolutionary paths to CAM than previously recognized.

36

37

38

39

40

41

42

43

44

45

46 *Isoetes*, commonly known as quillworts, is the only genus in the lycophyte order
47 Isoetales, containing roughly 250 described species¹. It is the last remaining member of an
48 ancient lineage with a fossil record that dates back to at least the late Devonian. As such,
49 quillworts are believed to represent the closest living relatives of the giant, tree-like lycopsids
50 such as *Sigillaria* and *Lepidodendron* that dominated the terrestrial landscape during the
51 Carboniferous². However, in contrast to its arborescent ancestors, modern *Isoetes* species are
52 diminutive and mostly aquatic with the vast majority of species growing completely or partially
53 submerged. Underwater, *Isoetes* can conduct CAM³, a carbon concentrating mechanism
54 involving the separation of carbon uptake and fixation in a time of day (TOD) fashion, with
55 carbon being sequestered as malate at night, to be fed into the Calvin cycle during the day.
56 CAM is a common strategy to improve water-use efficiency among xeric-adapted plants,
57 allowing them to keep their stomata closed during the day. However, its prevalence in aquatic
58 species of *Isoetes*³, as well as several aquatic angiosperms^{4,5}, suggests that it must have some
59 utility unrelated to conserving water. Specifically, it is thought to be an adaptation to low aquatic
60 CO₂ availability in the oligotrophic lakes and seasonal pools where *Isoetes* species are
61 commonly found^{4,6}.

62 Though it has been nearly four decades since Keeley first described “CAM-like diurnal
63 acid metabolism” in *Isoetes howellii*⁷, relatively little is known about the genetic mechanisms
64 controlling CAM in *Isoetes* or any other aquatic plant. Previous genomic and/or transcriptomic
65 studies that focused on terrestrial CAM have found evidence for regulatory neofunctionalization,
66 enrichment of cis-regulatory elements, and/or reprogramming of gene regulatory networks that
67 underlie the convergent evolution of CAM in *Sedum album*⁸, *Ananas comosus*⁹, *Kalanchoe*
68 *fedtschenkoi*¹⁰, several orchids^{11–13}, and Agavoideae species^{14,15}. Furthermore, a remarkable
69 case of amino acid sequence convergence in phosphoenolpyruvate carboxylase (PEPC), which
70 catalyzes the carboxylation of phosphoenolpyruvate (PEP) to yield oxaloacetate (OAA), has
71 also been reported among terrestrial CAM plants¹⁰. However, the lack of a high-quality genome
72 assembly has made meaningful comparison of *Isoetes* or any other aquatic CAM plant to
73 terrestrial CAM species impossible.

74 The only lycophyte genomes available to date are from the genus *Selaginella*^{16–18},
75 leaving a deep, >300-million-year gap in our knowledge of lycophyte genomics and limiting
76 inferences of tracheophyte evolution. *Selaginella* is the only genus in the Selaginellales, the
77 sister clade to Isoetales. Notably, *Selaginella* is known for being one of few lineages of vascular
78 plants for which no ancient whole genome duplications (WGDs) have been detected.
79 Conversely, there is evidence from transcriptomic data for as many as two rounds of WGD in
80 *Isoetes tegetiformans*¹⁹. As such, a thorough characterization of the history of WGD in *Isoetes* is
81 vital to future research into the effects and significance of WGD in lycophytes as a whole.

82 With this study we sought to investigate genome evolution as well as the genetic
83 underpinnings of CAM in *Isoetes*. To that end, we present a high-quality genome assembly for
84 *Isoetes taiwanensis*. To our knowledge, this is not only the first such assembly for the order
85 Isoetales, but also the first for an aquatic CAM plant. We found evidence for a single ancient
86 WGD event that appears to be shared among multiple species of *Isoetes*. Additionally, while
87 many CAM pathway genes display similar expression patterns in *Isoetes* and terrestrial
88 angiosperms, notable differences in gene expression suggest that the evolution of CAM may
89 have followed very different trajectories in these highly divergent groups.

90 **Results and Discussion:**

91 ***Genome assembly, annotation, and organization***

92 Using Illumina short-reads, Nanopore long-reads, and Bionano optical mapping, 90.13%
93 of the diploid ($2n = 2x = 22$ chromosomes) *I. taiwanensis* genome was assembled into 204
94 scaffolds (N50=17.40 Mb), with the remaining 9.87% into 909 unplaced contigs (Table 1). The
95 total assembled genome size (1.66 Gb) is congruent with what was estimated by K-mers (1.65
96 Gb) and flow cytometry (1.55 Gb) (Supplementary Fig. S1). A circular-mapping plastome was
97 also assembled, from which we identified a high level of RNA-editing (Supplementary Notes,
98 Supplementary Fig. S2).

99 A total of 39,461 high confidence genes were annotated based on *ab initio* prediction,
100 protein homology, and transcript evidence. The genome and proteome BUSCO scores are
101 94.5% and 91.0% respectively, which are comparable to many other seed-free plant genomes
102 (Supplementary Fig. S3) and indicative of high completeness. Orthofinder²⁰ analysis of 25
103 genomes placed 647,535 genes into 40,144 orthogroups. Subsequent analysis of key stomatal
104 and root genes in *I. taiwanensis* genome supported their homology (at the molecular level) with
105 similar structures in other vascular plants. In addition, examination of lignin biosynthesis genes
106 in *I. taiwanensis* suggests that evolution of a novel pathway to S-lignin likely predates the
107 divergence of *Isoetes* and *Selaginella*. A detailed discussion of these analyses and Orthofinder
108 results can be found in the Supplementary Notes and Supplementary Figures S4-S20.

109 Repetitive sequences accounted for 38% of the genome assembly with transposable
110 elements (TEs) accounting for the majority of those at 37.08% of the assembly length. Long
111 terminal repeat (LTR) retrotransposons were the most abundant (15.72% of total genome
112 assembly) with the Gypsy superfamily accounting for around 68% of LTR coverage (10.7% of
113 total genome assembly; Supplementary Table 1). When repeat density was plotted alongside
114 gene density, the distribution of both was found to be homogeneous throughout the assembly
115 (Fig. 1). This even distribution of genes and repeats is markedly different from what has been
116 reported in most angiosperm genomes²¹ where gene density increases near the ends of
117 individual chromosomes, but consistent with several high-quality genomes published from seed-
118 free plants, including *Physcomitrium patens*²², *Marchantia polymorpha*²³, and *Anthoceros*
119 *agrestis*²⁴. The result from *I. taiwanensis* thus adds to the growing evidence that the genomic
120 organization might be quite different between seed and seed-free plants²⁵.

121

122 **Table 1. *Isoetes taiwanensis* genome assembly statistics.**

Assembly size (Mb)	1,658.30
Scaffolds (#)	204
Scaffold length (Mb)	1494.58
N50 of scaffold length (Mb)	17.40
Scaffolded contigs (#)	1,879
Scaffolded contig length (Mb)	1211.25
N50 length of scaffolded contigs (Mb)	1.48
Unscaffolded contig (#)	909

Unscaffolded contig (Mb)	149.46
N50 length of unscaffolded contigs (Mb)	0.26
Genome BUSCO score (Eukaryota) (%)	94.5
Proteome BUSCO score (Eukaryota) (%)	91.0
Predicted protein coding genes (#)	39,461
Predicted repetitive sequence (%)	38

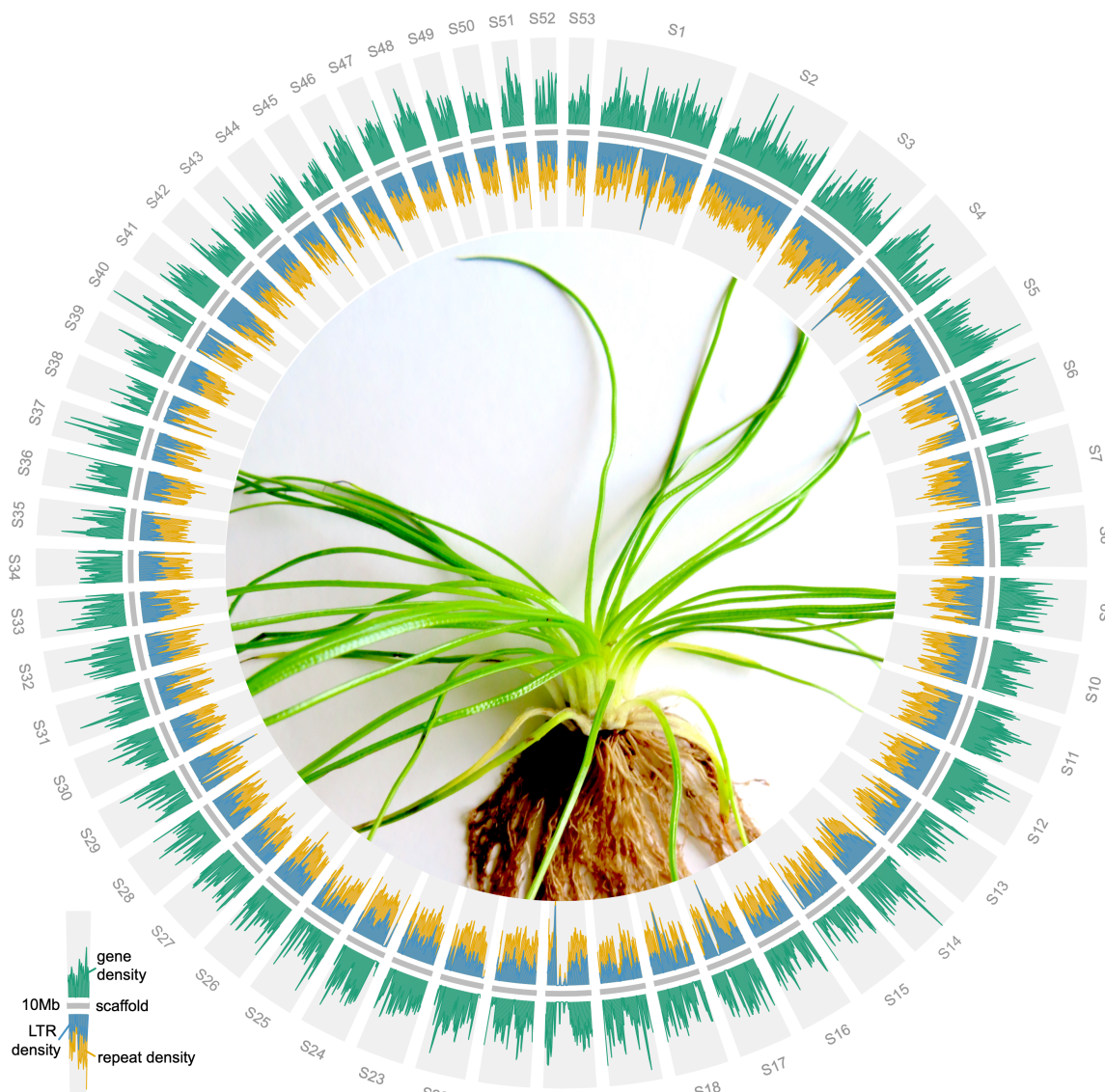


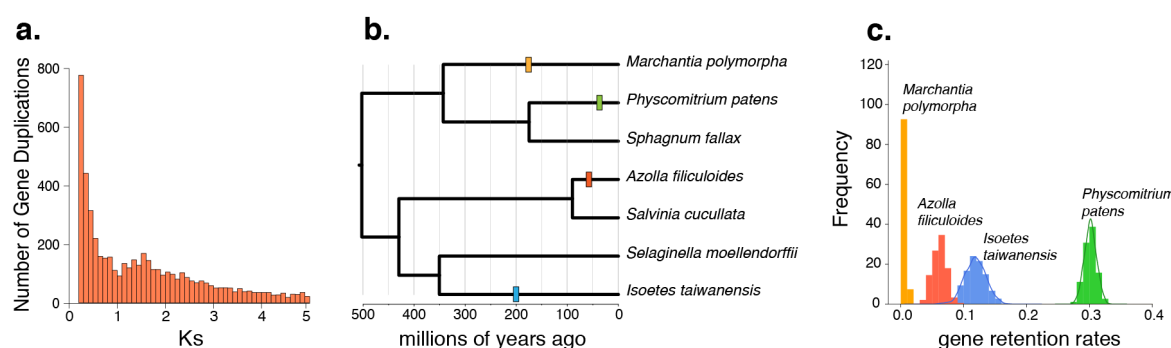
Fig 1: Distribution of genes and repetitive elements in *I. taiwanensis*. The relatively even distributions differ from angiosperm genomes, but are similar to what have been reported in other seed-free plants. Only scaffolds longer than 10 Mb are plotted. Center: an image of *I. taiwanensis*.

123
124
125
126
127
128
129
130

131 **Evidence for WGD in *Isoetes taiwanensis***

132 Using a combination of methods including synonymous substitutions per site (Ks),
133 phylogenetic, and synteny analyses, we identified a single ancient WGD in *I. taiwanensis*. This
134 is in contrast to a previous Ks analysis using 1KP transcriptome data, which found evidence for
135 two rounds of WGD, named ISTE α and ISTE β , in the North American species *I. tegetiformans*
136 and *I. echinospora*²⁶. These two WGDs have median Ks values of ~0.5 and ~1.5²⁶
137 (Supplementary Figure S21). Our whole paratome analysis of Ks in *I. taiwanensis* revealed a
138 single peak at Ks ~ 1.8 (Fig. 1a), suggesting that the earlier of the two duplications (ISTE β) in *I.*
139 *tegetiformans* and *I. echinospora* is shared by *I. taiwanensis* while the more recent event
140 (ISTE α) is not. Further analysis of orthologous divergence between *I. taiwanensis* and *I.*
141 *lacustris* indicated that ISTE β predates the divergence of these two species (Supplementary
142 Figure S22). The ISTE β event was subsequently confirmed by gene tree-species tree
143 reconciliation using genomic data in the WhALE package²⁷. WhALE returned a posterior
144 distribution of gene retention centered on $q = \sim 0.12$. This result compares favorably with a
145 previously documented WGD event in *Azolla filiculoides*²⁸ ($q = \sim 0.08$) and is in stark contrast to
146 our negative control, *Marchantia polymorpha*²³ ($q = \sim 0$) (Fig. 2b,c).

147 While self-self synteny analysis revealed 6,196 genes (15.7%) with a syntenic depth of
148 1x in 107 clusters (Supplementary Figure S23), we do not believe they resulted from WGD. Our
149 Ks analysis restricted to syntenic gene pairs failed to recover the peak at Ks ~1.8 and instead
150 consisted of an initial slope toward a much lower Ks value (Supplementary Figure S24).
151 Considering their high degree of similarity and location on separate scaffolds, it is possible that
152 these low Ks gene pairs are the result of relatively recent segmental duplications. The absence
153 of synteny from ISTE β is unsurprising. The high Ks value implies that ISTE β is quite ancient;
154 long enough ago for extensive genomic restructuring and fractionation to have taken place.
155 Altogether, of the two hypothesized WGDs in *Isoetes*, we confirmed the presence of ISTE β
156 while the younger ISTE α might be either specific to *I. tegetiformans* and *I. echinospora* or an
157 artifact stemming from the quality or completeness of the transcriptomes.



159 **Fig. 2: Evidence for WGD in *I. taiwanensis*.** a, Ks plot showing a peak centered on 1.8 corresponding to the ISTE β
160 event. b, Hypothesized WGD events that were tested (colored rectangles) in our WhALE analysis are shown on a
161 phylogeny. c, *I. taiwanensis*' posterior distribution of gene retention rates falls between that of *A. filiculoides* and *P.*
162 *patens*, both are known to have at least one WGD. This provides additional support for the ISTE β event. Conversely,
163 the gene retention rate is close to zero for *M. polymorpha*, consistent with its lack of WGD.

164
165
166
167

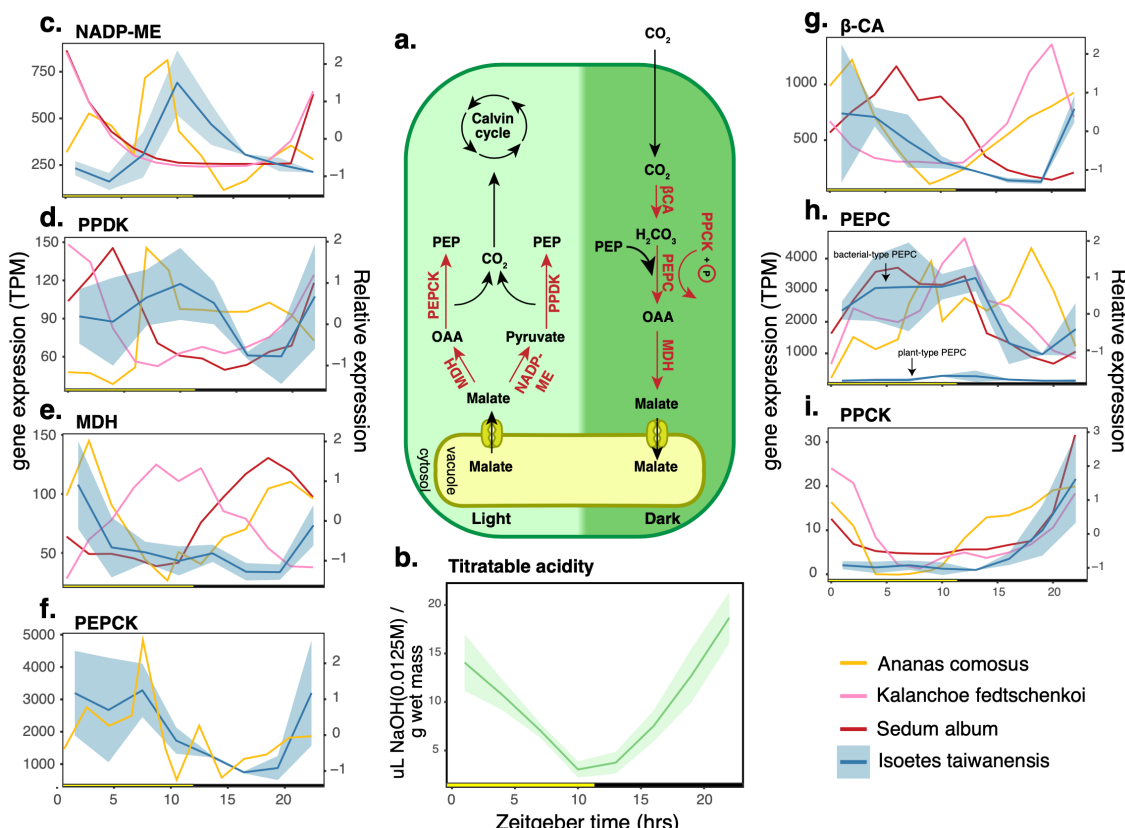
168 **Similarities to terrestrial CAM plants**

169 As a lycophyte, *Isoetes* represents the oldest extant lineage of vascular plants to exhibit
170 CAM photosynthesis (Fig 3a), and may be considered unusual among other CAM plants due to
171 its aquatic lifestyle. Here, we demonstrated that when submerged, titratable acidity in the leaves
172 of *I. taiwanensis* increased throughout the night, reaching peak acidity in the morning and
173 decreased throughout the daylight hours (Fig 3b), consistent with the cycle of carbon
174 sequestration and assimilation seen in dry-adapted CAM plants. To identify the underlying
175 genetic elements, we generated TOD RNA-seq, sampling every 3 hours over a 27-hour period
176 under 12 h light/12 h dark and continuous temperature (LDHH). A multidimensional scaling
177 (MDS) plot of normalized expression data showed that the samples were generally clustered in
178 a clockwise fashion as expected for TOD expression analysis (Supplemental Figure S25).

179 We found that some of the CAM pathway genes in *I. taiwanensis* exhibited TOD
180 expression patterns that largely resemble those found in terrestrial CAM plants (Fig. 3c-i). For
181 example, the strong dark expression of *PHOSPHOENOLPYRUVATE CARBOXYLASE KINASE*
182 (*PPCK*) appears to be conserved in *I. taiwanensis* as well as in all three terrestrial taxa (Fig 3i).
183 Likewise, we found one copy of *β-CARBONIC ANHYDRASE* (*β-CA*) that cycled similarly with
184 homologs in *A. comosus* and *K. fedtschenkoi* (Fig. 3g)—increasing during the night and peaking
185 in early morning—although this is different from *S. album* in which no *β-CA* genes showed a
186 high dark expression. Similar to *A. comosus* where two copies of *MALATE DEHYDROGENASE*
187 (*MDH*) were found to cycle in green leaf tissue⁹, we found multiple copies of *MDH* that appear to
188 cycle in *I. taiwanensis* with one copy appearing to exhibit similar peak expression to its
189 orthologue in pineapple (Fig. 3e). However, neither of the other two *MDH* genes that cycle in *I.*
190 *taiwanensis* exhibit similar expression to their orthologues in terrestrial CAM species
191 (Supplementary Figure S26).

192 During the day, decarboxylation typically occurs by one of two separate pathways (Fig.
193 3a). The first utilizes *NAPD-MALIC ENZYME* (*NADP-ME*) and *PYRUVATE PHOSPHATE*
194 *DIKINASE* (*PPDK*), and appears to be favored by *K. fedtschenkoi* and *S. album*^{8,10}. The second
195 utilizes *MDH* and *PHOSPHOENOLPYRUVATE CARBOXYKINASE* (*PEPCK*) and is favored by
196 *A. comosus*⁹. Based on its TOD expression of multiple copies of *MDH* and associated
197 expression dynamics, it is possible that *I. taiwanensis* utilizes the *MDH/PEPCK* pathway. While
198 all four genes have elevated expression levels during the day, the expression of *NADP-ME* is
199 inverted compared to *K. fedtschenkoi* and *S. album* (Fig. 3c), and *PPDK* exhibits relatively weak
200 cycling overall (R=0.637; Fig. 3d). Additionally, *PEPCK* and one copy of *MDH* have similar TOD
201 expression in *I. taiwanensis* and *A. comosus* (Fig. 3f and 3e, respectively), which may indicate a
202 shared affinity for *MDH/PEPCK* decarboxylation. Interestingly, the copy of *PEPCK* that cycles in
203 *I. taiwanensis* is not orthologous to the copy that cycles in *A. comosus*, being placed in a
204 different orthogroup by Orthofinder²⁰.

205
206
207



208
209
210
211
212
213
214

Fig. 3: Key CAM pathway genes and their expression patterns in *I. taiwanensis*. **a**, The CAM pathway with important reactions and their enzymes shown in red. **b**, Titratable acidity in *I. taiwanensis* exhibited a clear diel fluctuation. Diel expression patterns for highlighted genes are shown for the day (**c-f**) and night reactions (**g-i**). Average of TPM normalized expression data for *I. taiwanensis* is plotted in blue with a shaded ribbon representing the standard deviation (left y-axis). Relative expression profiles for homologous, cycling genes in other CAM species are plotted for comparison (right y-axis). All times are displayed in hours after lights-on (Zeitgeber time).

215

I. taiwanensis has recruited bacterial-type PEPC

216 While TOD expression of many key CAM pathway genes was broadly similar to that seen
217 in terrestrial CAM plants, one important difference can be found in the PEPC enzyme, which is
218 the entry point of carboxylation in CAM and C4 photosynthesis (Fig. 3a). PEPC is present in all
219 photosynthetic organisms as well as many non-photosynthetic bacteria and archaea. It is a vital
220 component of plant metabolism, carboxylating PEP in the presence of HCO_3^- to yield OAA. In
221 plants, the *PEPC* gene family consists of two clades, the “plant-type” and the “bacterial-type.”
222 The latter was named because of its higher sequence similarity with proteobacteria *PEPC* than
223 other plant-type *PEPC* genes²⁹. All CAM and C4 plants characterized to date recruited only the
224 plant-type *PEPC*³⁰, with the bacterial-type often being expressed at relatively low levels and/or
225 primarily in non-photosynthetic tissues³¹.

226 Interestingly, in *I. taiwanensis* we found that both types of *PEPC* were cycling and that the
227 bacterial-type was expressed at much higher levels than plant-type *PEPC* (Fig. 3h). Copies from
228 both types had similar expression profiles in *I. taiwanensis*, peaking at dusk and gradually
229 tapering off during the night. While this may seem counterintuitive as *PEPC* is an important
230 component of the dark reactions, it is consistent with what has previously been found in other
231 terrestrial CAM plants, with the overall expression profile resembling that of *S. album*⁸. The

233 advantage of recruiting bacterial-type PEPC is unclear. *In vivo*, both bacterial- and plant-type
234 PEPC can interact with each other to form a hetero-octameric complex that is less sensitive to
235 inhibition by malate³². Although the functional and physiological implications await future
236 studies, the unusual involvement of bacterial-type PEPC speaks to the uniqueness of *Isoetes'*
237 underwater CAM.

238

239 **No evidence for convergent evolution of PEPC**

240 Plant-type PEPC was recently shown to undergo convergent amino acid substitutions in
241 concert with the evolution of CAM¹⁰. An aspartic acid (D) residue appears to have been
242 repeatedly selected across multiple origins of CAM such as in *K. fedtschenkoi* and *P. equestris*,
243 although notably not in *A. comosus*¹⁰. This residue is situated near the active site, and based on
244 *in vitro* assays, the substitution to aspartic acid significantly increased PEPC activity¹⁰. However,
245 in *I. taiwanensis* we did not observe the same substitution in any copies of PEPC (Fig. 4);
246 instead, they have arginine (R) or lysine (H) at this position like PEPC from many non-CAM
247 plants. This lack of sequence convergence between *Isoetes* and flowering plants could be the
248 result of their substantial phylogenetic distance and highly divergent life histories. Alternatively,
249 it is also likely that the substitution is relevant only in the context of plant-type PEPC, and as *I.*
250 *taiwanensis* recruited the bacterial-type PEPC, the aspartic acid residue might not serve the
251 same purpose.

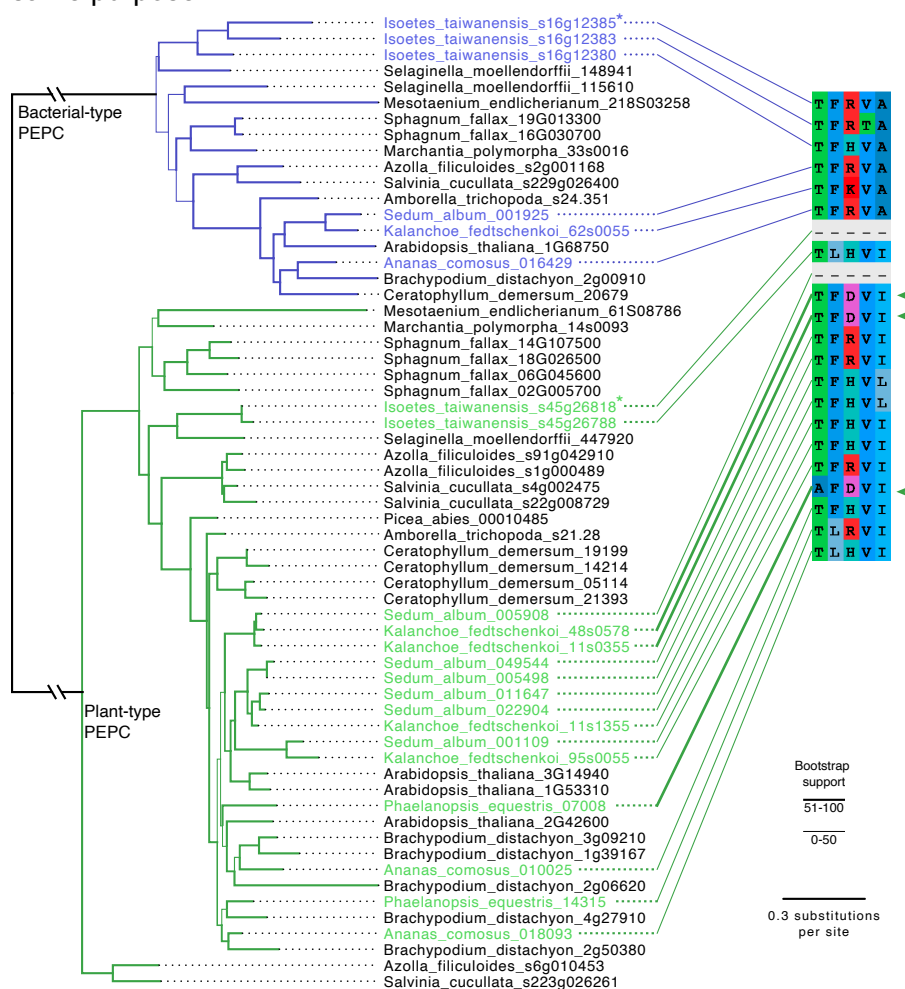


Fig. 4: A lack of PEPC sequence convergence in *I. taiwanensis*. Copies with putative convergent amino acid sequence (D at position 3 in alignment) are indicated by thickened connecting lines and green arrows. Copies of bacterial-type and plant-type PEPC shown to cycle in *I. taiwanensis* are marked with asterisks (*). Branch thickness indicates bootstrap support.

253 **A unique circadian regulation in Isoetes**

254 Previous analysis of the *A. comosus* genome found promoter regions of multiple key
255 CAM pathway genes containing known circadian cis-regulatory elements (CREs) including
256 Morning Element (ME: CCACAC), Evening Element (EE: AAATATCT), CCA1-binding site (CBS:
257 AAAATCT), G-box (CACGTG) and TCP15-binding motif (NGGNCCAC)⁹. This suggests that
258 expression of CAM genes in pineapple is largely under the control of a handful of known
259 circadian clock elements. The direct involvement of circadian CREs was corroborated by a later
260 study of the facultative CAM plant *S. album* where shifts in diel expression patterns were tied to
261 a shift in TOD-specific enrichment of CREs: EE and
262 Telobox (TBX: AAACCCT)⁸.

263 In order to examine the role of the circadian
264 clock and light/dark cycles in regulating *I. taiwanensis*
265 CAM, we used the HAYSTACK pipeline³³ to identify all
266 genes with TOD expression patterns. We predicted
267 3,241 cycling genes, which is 10% of the expressed
268 genes. While 10% is low compared to land plants that
269 have been tested under this condition (LDHH)—
270 usually at 30-50% genes^{8,33,34}, a recent study found a
271 reduced number of cycling genes in another aquatic
272 plant *Wolffia australiana* (duckweed/watermeal)³⁵.
273 Accordingly, decreased cycling may be a feature of
274 aquatic plants.

275 Core circadian clock genes such as *LATE*
276 *ELONGATED HYPOCOTYL* (*LHY*; Fig. 5a),
277 *PSEUDO-RESPONSE REGULATOR 7* (*PRR7*), *LUX*
278 *ARRHYTHMO* (*LUX*), and *EARLY FLOWERING 3*
279 (*ELF3*) (Supplementary Figure S27), cycle with the
280 expected TOD expression seen in their *Arabidopsis*
281 orthologs³³. However, *ZEITLUPE* (*ZTL*) does not
282 appear to cycle in *I. taiwanensis*, in contrast to
283 orthologues in *Arabidopsis* and *Selaginella*³⁶.
284 Furthermore, *TIMING OF CAB2 1/PSEUDO-*
285 *RESPONSE REGULATOR 1* (*TOC1/PRR1*) and
286 *GIGANTEA* (*GI*), which are typically single-copy genes
287 in land plants, have respectively 3 and 5 predicted
288 genes in distinct genomic locations; similarly an
289 increased number of homologs was found in the
290 facultative CAM plant *S. album*⁸. Closer inspection
291 confirmed all 3 *TOC1/PRR1* paralogs are full length,
292 while only 1 of the *GI* genes (*GIa*) is full length and 1
293 other (*GIb*) is a true partial/truncated (and expressed)
294 paralog. Surprisingly, all 3 copies of *TOC1/PRR1* have
295 dawn-specific expression compared to the dusk-specific
296 expression found in all plants tested to date³⁷ (Fig. 5b).

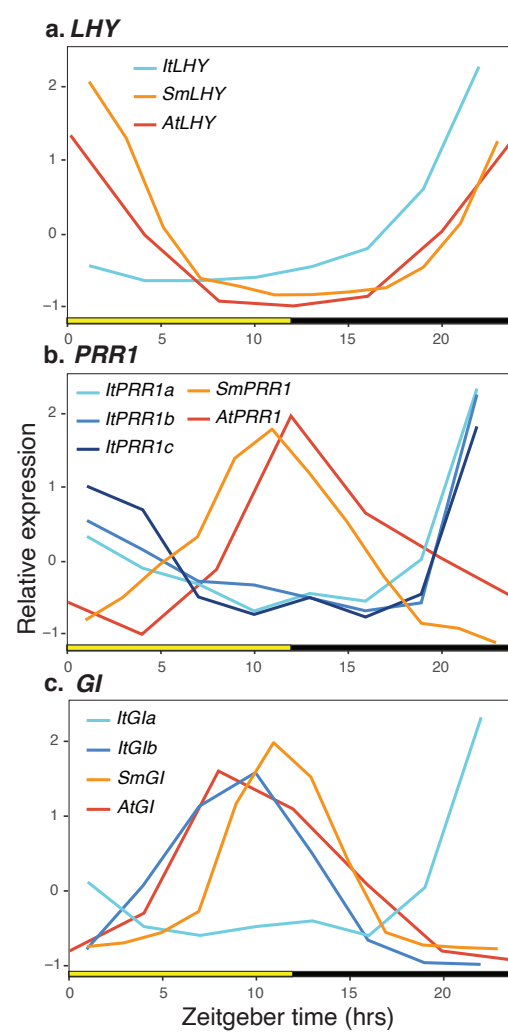


Fig. 5: Expression of key circadian associated genes is shifted in *I. taiwanensis*. a, *LATE ELONGATED HYPOCOTYL* (*LHY*) (CCA1), b, *PSEUDO-RESPONSE REGULATOR 1* (*PRR1*), and c, *GIGANTEA* (*GI*) orthologs in *Isoetes* (blue lines), *Selaginella* (orange line) and *Arabidopsis* (red line) over the day. Day (yellow box); Night (black box); Zeitgeber time (ZT) is the number of hours (hrs) after lights-on (0 hrs).

297 In addition, *Gla* and *Glb* have antiphasic expression, with the full length *Gla* having dusk-
298 specific expression, which is consistent with other plants, and *Glb* having dawn-specific
299 expression (Fig. 5c).

300 The duplications and divergent expression patterns of *TOC1/PRR1* and *GI* in *I.*
301 *taiwanensis* have important implications on circadian clock evolution. Despite the TOD
302 expression of core circadian clock genes being highly conserved since the common ancestor of
303 green algae and angiosperms, the mechanisms may be simpler in algae³⁸ and mosses³⁹. This is
304 largely due to a lack of key components of the evening-phased loop including *PRR1*, *GI*, and
305 *ZTL* in *P. patens* and the absence of the same along with morning-phased loop genes *ELF3*
306 and *ELF4* in algae³⁶. While *I. taiwanensis* possesses all the major clock genes that are found in
307 other vascular plants, lineage specific expansion and phase-shifted gene expression in the
308 evening-phased loop could indicate that circadian control was less conserved during the early
309 evolution of land plants. However, *Selaginella* exhibits very similar expression of various
310 circadian modules relative to other vascular plants and likewise, possesses a single copy of
311 both *GI* and *PRR1*³⁶. It is thus possible that the unique TOD architecture in *I. taiwanensis*
312 represents a more recent adaptation to its aquatic CAM lifestyle. As a comparison, *S. album*
313 similarly has multiple duplicated clock genes and its transition to CAM is associated with
314 significant shifts in both phase and amplitude of gene expression⁸. To further investigate the
315 relationship between clock and CAM in *I. taiwanensis*, we next focused on characterizing the
316 circadian CREs.

317

318 **Canonical circadian CREs are not enriched in Isoetes CAM cycling genes**

319 We used ELEMENT³³ to exhaustively search the promoter region of cycling genes for
320 putative CRE motifs. Following *de novo* identification, putative CREs were compared to known
321 transcription factor binding sites in *Arabidopsis* to determine to what degree their functions
322 might be conserved between *Isoetes* and flowering plants. We identified 16 significantly
323 enriched CREs motifs in the 500 bp 5' promoter region of cycling genes identified by
324 HAYSTACK, and clustered them according to TOD expression (Supplementary Table S3). Half
325 of the motifs shared some degree of sequence similarity to known circadian CREs previously
326 identified in *Arabidopsis*, including the EE as well as two 'ACGT'-containing elements (Gbox-
327 like) and two TBX-containing motifs³³. In the case of TBX, both motifs were associated with
328 peak expression at dusk (at around 12 hrs after lights on; Zeitgeber Time [ZT]) in *I. taiwanensis*
329 (Fig. 6a,b), similar to *Arabidopsis* under light/dark cycles alone³³. On the other hand, the EE
330 appear to be associated with peak expression at different TOD. In *Arabidopsis*, the EE is
331 enriched in genes with peak expression at dusk (ZT = 12), but in *I. taiwanensis*, this pattern is
332 shifted, with the EE associating with genes that peak in expression around mid-day (ZT= 6)
333 (Fig. 6c). Additionally, while the two 'ACGT'-containing elements were found upstream of genes
334 that exhibited significant cycling behavior, neither was strongly associated with peak expression
335 at a particular TOD. We also found an unidentified CRE (AGAATAAG) strongly associated with
336 peak expression in the morning (ZT = 4)(Fig. 6d).

337 We next examined the connection between circadian CREs and CAM genes in *I.*
338 *taiwanensis*. Interestingly, with the exception of the RVE1/2 motif, we did not find significant
339 enrichment of any known circadian CREs in CAM cycling genes relative to non-cycling
340 paralogues. While a targeted search of CAM cycling gene promoters did uncover circadian

341 CREs including the CBS, TCP15, TBX, and EE
342 (Supplementary Table S4), none were strongly
343 associated with either light or dark phase CAM gene
344 expression. In addition, both ME and G-box were
345 conspicuously absent from the promoter regions of
346 cycling CAM photosynthetic genes.

347 In sum, TOD-specific enrichment of CREs
348 appears to differ significantly from *Arabidopsis*. While
349 some CRE sequences themselves are conserved
350 between lycophytes and angiosperms, their interaction
351 with various transcription factors and subsequent
352 regulatory function could be quite different in *Isoetes*.
353 Importantly, our results stand in contrast to other CAM
354 plants such as *S. album*⁸ and *A. comosus*⁹ where CAM
355 genes appeared to be under the direct control of a
356 handful of strictly conserved circadian CREs. These
357 results either suggest that the circadian clock network
358 that emerged in *Isoetes*, which included the addition of
359 central components *GI* and *PRR1*, was quite different
360 than that found to be highly conserved in seed plants, or
361 there is significant TOD innovation associated with the
362 evolution of underwater CAM. Additional *Isoetes*
363 genomes and TOD analysis of underwater CAM plants
364 will be required to narrow these hypotheses.
365

366 Conclusion

367 The assembly and analyses of the *I. taiwanensis*
368 genome bridges a substantial gap in our knowledge of
369 vascular plant evolution. We have combined genomic
370 and transcriptomic data to corroborate one of the two
371 hypothesized WGDs in *Isoetes* relative to its closest
372 extant relative *Selaginella*, highlighting the contrasting
373 history of WGD in these two lineages. Importantly,
374 comparison of TOD gene expression with genomic
375 sequence data has given us unique insights into the
376 convergent evolution of CAM photosynthesis, not only in
377 a lycophyte, but also in the aquatic environment. As
378 such, our analysis stands as a necessary counterpoint to similar studies previously conducted in
379 terrestrial angiosperms. Shifts in expression of CAM pathway genes and the recruitment of
380 bacterial-type PEPC in *I. taiwanensis* demonstrate a remarkable degree of plasticity in the
381 convergent evolution of this complex trait throughout vascular plants. Likewise, differences in
382 the enrichment of CREs associated with circadian gene expression suggest that control of CAM,
383 as well as other processes tied to the circadian clock, may have diverged significantly since the
384 common ancestor of *Isoetes* and flowering plants. We propose that the emergence of

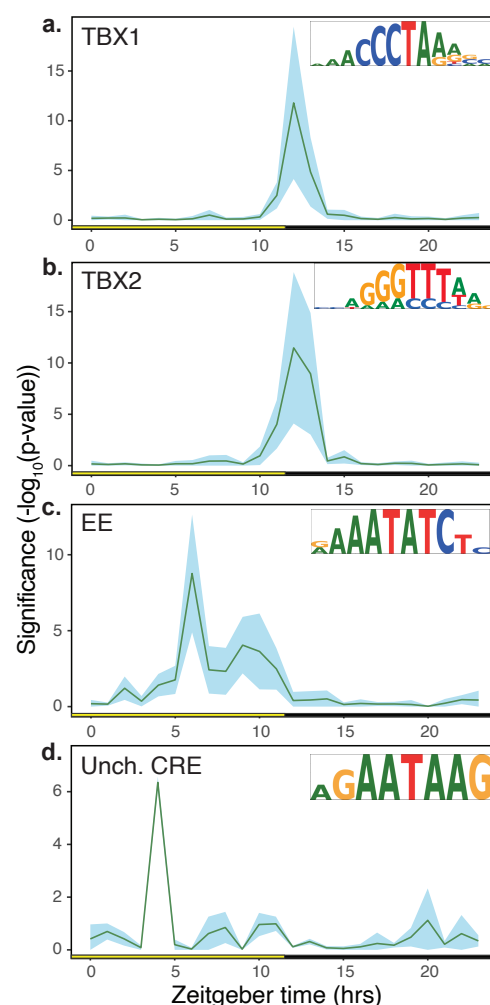


Fig. 6: Multiple CREs exhibit time-structured enrichment in *I. taiwanensis*.
a,b, Two telobox (TBX) containing motifs showed similar patterns to one another, both being enriched in genes with peak expression at dusk. c, A motif containing Evening Element (EE) was significantly enriched in genes with peak expression at mid-day. d, A novel motif was significantly enriched at mid-day as well. Day (yellow box); Night (black box); Zeitgeber time (ZT) is the number of hours (hrs) after lights on (0 hrs).

385 underwater CAM may have followed a distinct route in *Isoetes*, shedding new light on a classic
386 example of convergent evolution of a complex plant trait.

387

388 **Methods:**

389 **Plant sample**

390 *Isoetes taiwanensis* is endemic to a small pond in Northern Taiwan and has been *ex situ*
391 propagated in Taiwan Forestry Research Institute. This species is expected to have a low
392 genetic diversity due to a very restricted distribution and a small population size. The voucher
393 specimen was deposited at TAIF herbarium.

394

395 **Genome size estimate**

396 The genome size of *I. taiwanensis* was first determined by flow cytometry following the
397 protocols outlined in Kuo et al.⁴⁰ and Li et al²⁸. The flow cytometric experiments were performed
398 on BD FACSCan system (BD Biosciences, USA), and the Beckman buffer⁴¹ was used with
399 0.5% (v/v) 2-mercaptoethanol, 40 mg ml⁻¹ PVP-40, and 0.1 mg ml⁻¹ RNaseA added. We used
400 *Zea mays* (1C = 5.57pg⁴²) as the internal standard. To confirm the flow cytometry-based
401 measurement, a K-mer frequency distribution was generated from Illumina 2x150 bp paired
402 reads (described below) using Jellyfish⁴³, which was then input into GenomeScope⁴⁴ and an
403 inhouse pipeline to estimate genome size and heterozygosity.

404

405 **Genome sequencing**

406 High molecular weight (HMW) DNA was extracted using a modified CTAB method on
407 isolated nuclei. First, leaf tissues were ground in liquid nitrogen, and the powder was
408 resuspended in the Beckman buffer (same as in our flow cytometric experiments). We then
409 used 30µm nylon circular filters (Partec, Germany) to remove tissue debris, and precipitated
410 nuclei with 100g centrifugation under 4°C for 20 minutes. For the downstream CTAB
411 procedures, we followed the protocol outlined in Kuo⁴⁵. HMW DNA was QC'd on an agarose gel
412 for length and quantified on a bioanalyzer. Unsheared HMW DNA was used to make Oxford
413 Nanopore Technologies (ONT) ligation-based libraries (Oxford, UK). Libraries were prepared
414 starting with 1.5ug of DNA and following all other steps in ONT's SQK-LSK109 protocol. Final
415 libraries were loaded on an ONT flowcell (v9.4.1) and run on the GridION. Bases were called in
416 real-time on the GridION using the flip-flop version of Guppy (v3.1). The resulting fastq files
417 were concatenated and used for downstream genome assembly steps. The same batch of
418 HMW genomic DNA was used to construct Illumina (Illumina, USA) libraries for estimating
419 genome size (above) and correcting residual errors in the ONT assembly. Libraries were
420 constructed using the KAPA HyperPrep Kit (Kapa Biosystems, Switzerland) followed by
421 sequencing on an Illumina NovaSeq6000 with 2x150 bp paired-ends.

422

423 **Genome assembly**

424 ONT reads were assembled using minimap2 and miniasm⁴⁶, and the resulting draft
425 assembly was then polished by racon⁴⁷ (with nanopore reads) and pilon⁴⁸ (with Illumina reads).
426 Because the plants were grown non-axenically under water, the assembly inevitably contained
427 contaminations. We therefore used blobtools⁴⁹ to identify non-plant contigs based on a
428 combination of contig read coverage, taxonomic assignment, and GC content.

429 To further scaffold the assembly, we generated a genome map using Bionano with the
430 Direct Label and Stain chemistry and DLE-1 labeling. For this, high molecular weight DNA was
431 extracted using the Bionano Plant DNA Isolation Kit. Hybrid scaffolding, combining the
432 nanopore draft and Bionano map, was done on the Bionano Saphyr computing platform at the
433 McDonnell Genome Institute at Washington University. We then gap-filled the scaffolded
434 genome using two rounds of LR_Gapcloser⁵⁰ (3 iterations each and a pilon polishing in
435 between. Finally, to remove redundancy the purge_haplotype pipeline⁵¹ was used to obtain the
436 v1 assembly. The circular chloroplast genome was assembled from Illumina data using the
437 GetOrganelle⁵² toolkit.

438

439 **Repeat annotation**

440 We generated a custom *I. taiwanensis*-specific repeat library using LTR-retriever⁵³ and
441 RepeatModeler⁵⁴. To identify and remove repeats with homology to plant proteins, we used
442 BLASTx to query each repeat against the uniprot plant protein database (e-value threshold at
443 1e-10). The resulting library was then input into RepeatMasker⁵⁵ to annotate and mask the
444 repetitive elements in the *I. taiwanensis* genome.

445

446 **Gene annotation**

447 We trained two *ab initio* gene predictors, AUGUSTUS⁵⁶ and SNAP⁵⁷, on the repeat-
448 masked genome using a combination of protein and transcript evidence. For the protein
449 evidence, we relied on the annotated proteomes from *Selaginella moellendorffii*¹⁶ and *S.*
450 *lepidophylla*¹⁸, and for the transcript evidence, we used the RNA-seq data from our time-course
451 experiment and a separate corm sample. To train AUGUSTUS, BRAKER2⁵⁸ was used and the
452 transcript evidence was input as an aligned bam file. On the other hand, SNAP was trained
453 under MAKER with 3 Iterations, and in this case, the transcript evidence was supplied as a *de*
454 *novo* assembled transcriptome done by Trinity⁵⁹. After AUGUSTUS and SNAP were trained,
455 they were fed into MAKER⁶⁰ along with all the evidence to provide a synthesized gene
456 prediction. Gene functional annotation was done using the eggNOG-mapper v2⁶¹. To filter out
457 spurious gene models, we removed genes that met none of the following criteria: (1) a transcript
458 abundance greater than zero in any sample (as estimated by Stringtie⁶²), (2) has functional
459 annotation from eggNOG, and (3) was assigned into orthogroups in an Orthofinder²⁰ run (see
460 below). The resulting gene set was used in all subsequent analyses.

461

462 **Homology assessment and gene family analysis**

463 Homology was initially assessed with Orthofinder²⁰ using genomic data from a range of
464 taxa from across the plant tree of life including all CAM plant genomes published to date:
465 *Amborella trichopoda*⁶³, *Ananas comosus*⁹, *Anthoceros agrestis*²⁴, *Arabidopsis thaliana*⁶⁴, *Azolla*
466 *filiculoides*²⁸, *Brachypodium distachyon*⁶⁵, *Ceratophyllum demersum*⁶⁶, *Isoetes taiwanensis* (this
467 study), *Kalanchoe fedtschenkoi*¹⁰, *Marchantia polymorpha*²³, *Medicago truncatula*⁶⁷, *Nelumbo*
468 *nucifera*⁶⁸, *Nymphaea colorata*⁶⁹, *Phalaenopsis equestris*¹¹, *Physcomitrium patens*²², *Picea*
469 *abies*⁷⁰, *Salvinia cucullata*²⁸, *Sedum album*⁸, *Selaginella moellendorffii*¹⁶, *Sphagnum fallax*
470 (*Sphagnum fallax* v0.5, DOE-JGI, <http://phytozome.jgi.doe.gov/>), *Spirodela polyrhiza*⁷¹,
471 *Utricularia gibba*⁷², *Vitis vinifera*⁷³, and *Zostera marina*⁷⁴, and one algal genome: *Mesotaenium*

472 *endlicherianum*⁷⁵. Following homology assessment, the degree of overlap between gene
473 families was assessed using the UpsetR⁷⁶ package in R.

474

475 **RNA editing analysis**

476 RNA-seq data was first mapped to combined nuclear and chloroplast genome
477 assemblies using HISAT2⁷⁷. The reads mapping to the chloroplast genome were extracted
478 using samtools⁷⁸. SNPs were called using the mpileup function in bcftools⁷⁹. The resulting vcf
479 files were filtered using bcftools to remove samples with a depth < 20, quality score < 20 and
480 mapping quality bias < 0.05. After filtering, C-to-U and U-to-C edits were identified using an
481 alternate allele frequency threshold of 10%. Finally, RNA editing sites were related to specific
482 genes using the intersect command in bedtools⁸⁰ and characterized using a custom python
483 script.

484

485 **Ks analysis**

486 Ks divergence was calculated by several different methods. Initially, a whole paralome
487 Ks distribution was generated using the 'wgd mcl' tool⁸¹. Self-synteny was then assessed in i-
488 Adhore and Ks values were calculated and plotted for syntenic pairs only using the 'wgd syn'
489 tool⁸¹. To conduct Ks analysis of related species, RNA-seq data was downloaded from the SRA
490 database for *Isoetes yunguiensis*, *I. sinensis*, *I. drummondii*, *I. echinospora*, *I. lacustris* and *I.*
491 *tegetiformans*. Transcriptomes were assembled using SOAPdenovo-Trans⁸² with a Kmer length
492 of 31. Next, for each *Isoetes* genome and transcriptome, we used the DupPipe pipeline to
493 construct gene families and estimate the age distribution of gene duplications^{83,84}. We translated
494 DNA sequences and identified ORFs by comparing the Genewise⁸⁵ alignment to the best-hit
495 protein from a collection of proteins from 25 plant genomes from Phytozome⁸⁶. For all DupPipe
496 runs, we used protein-guided DNA alignments to align our nucleic acid sequences while
497 maintaining the ORFs. We estimated Ks divergence using PAML⁸⁷ with the F3X4model for each
498 node in the gene family phylogenies. We then used mixture modeling to identify significant
499 peaks consistent with a potential WGD and to estimate their median paralog Ks values.
500 Significant peaks were identified using a likelihood ratio test in the boot.comp function of the
501 package mixtools⁸⁸ in R.

502

503 **Estimation of orthologous divergence**

504 To place putative WGDs in relation to lineage divergence, we estimated the synonymous
505 divergence of orthologs among pairs of species that may share a WGD based on their
506 phylogenetic position and evidence from the within-species Ks plots. We used the RBH
507 Orthologue pipeline⁸⁴ to estimate the mean and median synonymous divergence of orthologs,
508 and compared those with the synonymous divergence of inferred paleopolyploid peaks. We
509 identified orthologs as reciprocal best blast hits in pairs of transcriptomes. Using protein-guided
510 DNA alignments, we estimated the pairwise synonymous divergence for each pair of orthologs
511 using PAML⁸⁷ with the F3X4 model.

512

513 **Phylogenetic assessment of ancient whole genome duplication**

514 WGD inference was conducted by phylogenomic reconciliation using the WhALE
515 package implemented in Julia²⁷. First, prior to WhALE analysis, Orthofinder²⁰ was used to

516 identify groups of orthologous genes among 7 species representing 3 taxonomic groups
517 (bryophytes, lycophytes, and ferns): *Azolla filiculoides*²⁸, *Isoetes taiwanensis* (this study),
518 *Marchantia polymorpha*²³, *Physcomitrium patens*²², *Salvinia cucullata*²⁸, *Selaginella*
519 *moellendorffii*¹⁶, and *Sphagnum fallax* (*Sphagnum fallax* v0.5, DOE-JGI,
520 <http://phytozome.jgi.doe.gov/>). These species were chosen based on phylogenetic relatedness,
521 availability of a high-quality genome assembly, and previous assessment for the presence or
522 absence of WGD. The resulting orthogroups were filtered using a custom python script to
523 remove the 5% largest orthogroups and those with less than 3 taxa. Additionally, WhALE
524 requires removal of gene families that do not contain at least one gene in both bryophytes and
525 ferns to prevent the inclusion of gene families originating after divergence from the most recent
526 common ancestor. Alignments were generated for the filtered orthogroups in PRANK⁸⁹ using the
527 default settings. A posterior distribution of trees was obtained for each gene family in MrBayes
528 3.2.6⁹⁰ using the LG model. Chains were sampled every 10 generations for 100,000 generations
529 with a relative burn-in of 25%. Following the Bayesian analysis, conditional clade distributions
530 (CCDs) were determined from posterior distribution samples using ALEobserve in the ALE
531 software suite⁹¹. CCD files were subsequently filtered using the ccddata.py and ccdfilter.py
532 scripts provided with the WhALE program. A dated, ultrametric species tree was generated
533 using the 'ape' package in R⁹², in which branch lengths were constrained according to 95%
534 highest posterior density of ages, assuming that bryophytes are monophyletic, as reported by
535 Morris et al.⁹³. Finally, the filtered CCD files were loaded in Julia along with the associated
536 species phylogeny. A hypothetical WGD node was inferred at 200 million years ago (MYA)
537 along the branch leading to *I. taiwanensis*, prior to the estimated crown age of extant *Isoetes*⁹⁴.
538 Modifying the hypothetical age of this WGD node did not affect the outcome. Additional WGD
539 nodes were placed as positive controls along branches leading to *Physcomitrium patens* and
540 *Azolla filiculoides* at 40 MYA and 60 MYA, respectively, based on previous studies^{22,28}. A false
541 WGD event was also placed arbitrarily in *Marchantia polymorpha* at 160 MYA as a negative
542 control. A WhALE 'problem' was constructed using an independent rate prior and MCMC
543 analysis was conducted using the DynamicHMC library in Julia
544 (<https://github.com/tpapp/DynamicHMC.jl>) with a sample size of 1000.
545

546 **Phylogenetic analysis of root, stomata, and CAM pathway genes**

547 Following clustering of homologs in Orthofinder, we conducted phylogenetic analysis of
548 several gene families of interest, including those containing *SMF*, *FAMA*, *TMM*, *RSL*, and *PEPC*
549 genes, were subsequently identified based on homology using gene annotations from
550 *Arabidopsis*. Gene trees from Orthofinder were initially used to identify paralogues and remove
551 fragmented genes where appropriate. In the case of *PEPC*, orthogroups containing "bacterial-
552 type" and "plant-type" *PEPC* were combined prior to alignment. Next, amino acid sequences
553 were aligned using MUSCLE⁹⁵ under default settings and trimmed using TrimAL with the -strict
554 flag. An amino acid substitution model was selected according to the Bayesian Information
555 Criterion (BIC) in ModelFinder⁹⁶ prior to phylogenetic reconstruction by maximum likelihood in
556 IQ-TREE v1.6.12⁹⁷ with 1000 ultrafast⁹⁸ bootstrap replicates.
557

558 **Phylogenetic analysis of genes salient to the phenylpropanoid and lignin biosynthesis 559 pathway**

560 The datasets used for phylogenetic analysis were based on de Vries et al.⁹⁹ with added
561 *I. taiwanensis* sequences. In brief, we assembled a dataset of predicted proteins from (A) the
562 genomes of seventeen land plants: *Anthoceros agrestis* as well as *Anthoceros punctatus*²⁴,
563 *Amborella trichopoda*⁶³, *Arabidopsis thaliana*⁶⁴, *Azolla filiculoides*²⁸, *Brachypodium distachyon*⁶⁵,
564 *Capsella grandiflora*¹⁰⁰, *Gnetum montanum*¹⁰¹, *Isoetes taiwanensis* (this study), *Marchantia*
565 *polymorpha*²³, *Nicotiana tabacum*¹⁰², *Oryza sativa*¹⁰³, *Physcomitrium patens*²², *Picea abies*⁷⁰,
566 *Salvinia cucullata*²⁸, *Selaginella moellendorffii*¹⁶, and *Theobroma cacao*¹⁰⁴; (B) the genomes of
567 seven streptophyte algae: *Chlorokybus atmophyticus*¹⁰⁵, *Chara braunii*¹⁰⁶, *Klebsormidium*
568 *nitens*¹⁰⁷, *Mesotaenium endlicherianum*⁷⁵, *Mesostigma viride*¹⁰⁵, *Penium margaritaceum*¹⁰⁸,
569 *Spirogloea muscicola*⁷⁵—additionally, we included sequences found in the transcriptomes of
570 *Spirogyra pratensis*¹⁰⁹, *Coleochaete scutata* as well as *Zygnema circumcarinatum*¹¹⁰, and
571 *Coleochaete orbicularis*¹¹¹; (C) the genomes of eight chlorophytes: *Bathycoccus prasinos*¹¹²,
572 *Chlamydomonas reinhardtii*¹¹³, *Coccomyxa subellipsoidea*¹¹⁴, *Micromonas* sp. as well as
573 *Micromonas pusilla*¹¹⁵, *Ostreococcus lucimarinus*¹¹⁶, *Ulva mutabilis*¹¹⁷, *Volvox carteri*¹¹⁸. For
574 phenylalanine ammonia-lyase, additional informative sequences were added based on de Vries
575 et al.¹¹⁹.

576 Building on the alignments published in de Vries et al.⁹⁹, homologs of each gene family
577 (detected in the aforementioned species via BLASTp) were (re)-aligned using MAFFT v7.475¹²⁰
578 with a L-INS-I approach; both full and partial sequences from *I. taiwanensis* were retained. We
579 constructed maximum likelihood phylogenies using IQ-TREE 2.0.6¹²¹; 1000 ultrafast⁹⁸ bootstrap
580 replicates were computed. To determine the best model for protein evolution, we used
581 ModelFinder⁹⁶ and picked the best models based on BIC. Residue information was mapped
582 next to the tree based on structural analyses by Hu et al.¹²², Pan et al.¹²³, Louie et al.¹²⁴, Youn et
583 al.¹²⁵ and Ferrer et al.¹²⁶.

584

585 **Time course titratable acidity and RNA-seq experiments**

586 Leaves of *I. taiwanensis* were taken from five individuals every 3 hours over a 27-hour
587 period on a 12-hour light/dark cycle and constant temperature. To measure changes in acidity
588 over time, a portion of the leaf tissues was weighed, mixed with 3.5-5ml of ddH2O, and titrated
589 with 0.0125M NaOH solution until pH = 7.0. At the same time, we froze the leaf tissues in liquid
590 nitrogen, and extracted RNA using a modified CTAB protocol¹²⁷. RNA quality was examined on
591 a 1% agarose gel and RNA concentration was quantified using the Qubit RNA HS assay kit
592 (Invitrogen, USA). 2ug of total RNA was used to construct stranded RNA-seq libraries using the
593 Illumina TruSeq stranded total RNA LT sample prep kit (RS-122-2401 and RS-122-2402).
594 Multiplexed libraries were pooled and sequenced on an Illumina NovaSeq6000 with 2x150 bp
595 paired-ends.

596

597 **Differential expression analysis**

598 RNA-seq reads were mapped to the combined nuclear and chloroplast genome using
599 HISAT2⁷⁷. Stringtie⁶² was used to assemble transcripts and estimate transcript abundance. A
600 gene count matrix was produced using the included prepDE.py script. We imported gene count
601 data into the DESEQ2 package in R¹²⁸ for read normalization using its median of ratios method
602 as well as identification and removal of outlier samples using multidimensional scaling. A single
603 outlier sample from each of six time points (1hr, 4hrs, 7hrs, 10hrs, 13hrs and 19hrs) was

604 removed from the final dataset. The resulting dataset was used to analyze temporal gene
605 expression patterns in the R package maSigPro¹²⁹. Using maSigPro, genes with significantly
606 differential expression profiles were identified by computing a regression fit for each gene and
607 filtered based on the associated p-value (p<0.001).

608

609 ***HAYSTACK* global cycling prediction**

610 Genes with mean expression across all the time points below 1 TPM were considered
611 “not expressed” and filtered prior to cycling prediction with HAYSTACK
612 (https://gitlab.com/NolanHartwick/super_cycling)³³. HAYSTACK operates by correlating the
613 observed expression levels of each gene with a variety of user specified models that represent
614 archetypal cycling behavior. We used a model file containing sinusoid, spiking traces, and
615 various rough linear interpolations of sinusoids with periods ranging from 20 hours to 28 hours
616 in one-hour increments and phases ranging from 0-23 hours in one-hour increments. Genes
617 that correlated with their best fit model at a threshold of R > 0.8 were classified as cyclers with
618 phase and period defined by the best fit model. This threshold for calling cycling genes is based
619 on previous validated observations^{8,33,34,130}. We also validated this threshold by looking at the
620 cycling of known circadian clock genes (Fig. 5).

621

622 ***ELEMENT cis-regulatory elements analysis***

623 Once cycling genes in *I. taiwanensis* were identified, we were able to find putative cis-
624 acting elements associated with TOD expression. Promoters, defined as 500 bp upstream of
625 genes, were extracted for each gene and processed by ELEMENT (https://gitlab.com/salk-tm/snake_pip_element)^{33,131,132}. Briefly, ELEMENT generates an exhaustive background model
626 of all 3-7 K-mer using all of the promoters in the genome, and then compares the K-mers (3-7
627 bp) from the promoters for a specified gene list. Promoters for cycling genes were split
628 according to their TOD expression into “phase” gene lists and K-mers that were
629 overrepresented in any of these 24 promoter sets were identified by ELEMENT. By splitting up
630 cycling genes according to their associated phase, we gained the power to identify K-mers
631 associated with TOD-specific cycling behavior at every hour over the day. Our threshold for
632 identifying a K-mer as being associated with cycling was an FDR < 0.05 in at least one of the
633 comparisons. The significant K-mers were clustered according to sequence similarity (Fig. 6).

635

636 ***Promoter motif identification***

637 Core CAM genes with significantly differential diel expression profiles (as identified in
638 maSigPro) including *β-CA*, *PEPC*, *PEPCK*, *ME*, *MDH*, and *PPDK* were selected for motif
639 enrichment analysis. Enriched motifs were identified relative to a background consisting of non-
640 cycling paralogues of photosynthetic genes using the AME utility¹³³. Promoters were searched
641 for known motifs from the *Arabidopsis* promoter binding motif database¹³⁴ with FIMO¹³⁵.

642

643 ***Data availability:***

644 All the raw sequences were deposited in the NCBI Sequence Read Archive under the
645 BioProject PRJNA735564. Genome assembly and annotation are available at
646 <https://genomevolution.org/coge/GenomeInfo.pl?gid=61511>. Sequence alignments and tree files
647 can be found at https://github.com/dawickell/Isoetes_CAM.

648 **References:**

- 649 1. Pteridophyte Phylogeny Group I. A community-derived classification for extant lycophytes
650 and ferns. *J. Syst. Evol.* **54**, 563–603 (2016).
- 651 2. Pigg, K. B. Isoetalean lycopsid evolution: from the Devonian to the present. *Am. Fern J.* **91**,
652 99–114 (2001).
- 653 3. Keeley, J. E. Distribution of diurnal acid metabolism in the genus *Isoetes*. *Am. J. Bot.* **69**,
654 254–257 (1982).
- 655 4. Keeley, J. E. CAM photosynthesis in submerged aquatic plants. *Bot. Rev.* **64**, 121–175
656 (1998).
- 657 5. Aulio, K. Differential expression of diel acid metabolism in two life forms of *Littorella uniflora*
658 (L.) Aschers. *New Phytologist* **100**, 533–536 (1985).
- 659 6. Suissa, J. S. & Green, W. A. CO₂ starvation experiments provide support for the carbon-
660 limited hypothesis on the evolution of CAM-like behaviour in *Isoëtes*. *Ann. Bot.* **127**, 135–
661 141 (2021).
- 662 7. Keeley, J. E. *Isoetes howellii*: A submerged aquatic cam plant? *Am. J. Bot.* **68**, 420–424
663 (1981).
- 664 8. Wai, C. M. *et al.* Time of day and network reprogramming during drought induced CAM
665 photosynthesis in *Sedum album*. *PLOS Genetics* **15**, e1008209 (2019).
- 666 9. Ming, R. *et al.* The pineapple genome and the evolution of CAM photosynthesis. *Nat. Genet.* **47**,
667 1435–1442 (2015).
- 668 10. Yang, X. *et al.* The *Kalanchoë* genome provides insights into convergent evolution and
669 building blocks of crassulacean acid metabolism. *Nat. Commun.* **8**, 1899 (2017).
- 670 11. Cai, J. *et al.* The genome sequence of the orchid *Phalaenopsis equestris*. *Nat. Genet.* **47**,
671 65–72 (2015).
- 672 12. Zhang, L. *et al.* Origin and mechanism of crassulacean acid metabolism in orchids as
673 implied by comparative transcriptomics and genomics of the carbon fixation pathway. *Plant
674 J.* **86**, 175–185 (2016).
- 675 13. Heyduk, K. *et al.* Altered Gene Regulatory Networks Are Associated With the Transition
676 From C₃ to Crassulacean Acid Metabolism in *Erycina* (Oncidiinae: Orchidaceae). *Front.
677 Plant Sci.* **9**, 2000 (2018).
- 678 14. Heyduk, K. *et al.* Shared expression of crassulacean acid metabolism (CAM) genes pre-
679 dates the origin of CAM in the genus *Yucca*. *J. Exp. Bot.* **70**, 6597–6609 (2019).
- 680 15. Abraham, P. E. *et al.* Transcript, protein and metabolite temporal dynamics in the CAM
681 plant *Agave*. *Nat. Plants* **2**, 16178 (2016).
- 682 16. Banks, J. A. *et al.* The *Selaginella* genome identifies genetic changes associated with the
683 evolution of vascular plants. *Science* **332**, 960–963 (2011).
- 684 17. Xu, Z. *et al.* Genome analysis of the ancient tracheophyte *Selaginella tamariscina* reveals
685 evolutionary features relevant to the acquisition of desiccation tolerance. *Mol. Plant* **11**,
686 983–994 (2018).
- 687 18. VanBuren, R. *et al.* Extreme haplotype variation in the desiccation-tolerant clubmoss
688 *Selaginella lepidophylla*. *Nat. Commun.* **9**, 13 (2018).
- 689 19. One Thousand Plant Transcriptomes Initiative. One thousand plant transcriptomes and the
690 phylogenomics of green plants. *Nature* **574**, 679–685 (2019).
- 691 20. Emms, D. M. & Kelly, S. OrthoFinder: phylogenetic orthology inference for comparative
692 genomics. *Genome Biol.* **20**, 238 (2019).
- 693 21. Schmutz, J. *et al.* Genome sequence of the palaeopolyploid soybean. *Nature* **463**, 178–183
694 (2010).
- 695 22. Lang, D. *et al.* The *Physcomitrella patens* chromosome-scale assembly reveals moss
696 genome structure and evolution. *Plant J.* **93**, 515–533 (2018).
- 697 23. Diop, S. I. *et al.* A pseudomolecule-scale genome assembly of the liverwort *Marchantia*

698 *polymorpha*. *Plant J.* **101**, 1378–1396 (2020).

699 24. Li, F.-W. *et al.* Anthoceros genomes illuminate the origin of land plants and the unique
700 biology of hornworts. *Nat. Plants* **6**, 259–272 (2020).

701 25. Szövényi, P., Gunadi, A. & Li, F.-W. Charting the genomic landscape of seed-free plants.
702 *Nat. Plants* **7**, 554–565 (2021).

703 26. Li, Z. & Barker, M. S. Inferring putative ancient whole-genome duplications in the 1000
704 Plants (1KP) initiative: access to gene family phylogenies and age distributions.
705 *Gigascience* **9**, (2020).

706 27. Zwaenepoel, A. & Van de Peer, Y. Inference of Ancient Whole-Genome Duplications and
707 the Evolution of Gene Duplication and Loss Rates. *Mol. Biol. Evol.* **36**, 1384–1404 (2019).

708 28. Li, F.-W. *et al.* Fern genomes elucidate land plant evolution and cyanobacterial symbioses.
709 *Nat. Plants* **4**, 460–472 (2018).

710 29. Sánchez, R. & Cejudo, F. J. Identification and expression analysis of a gene encoding a
711 bacterial-type phosphoenolpyruvate carboxylase from *Arabidopsis* and rice. *Plant Physiol.*
712 **132**, 949–957 (2003).

713 30. Deng, H. *et al.* Evolutionary history of PEPC genes in green plants: Implications for the
714 evolution of CAM in orchids. *Mol. Phylogenet. Evol.* **94**, 559–564 (2016).

715 31. Ting, M. K. Y., She, Y.-M. & Plaxton, W. C. Transcript profiling indicates a widespread role
716 for bacterial-type phosphoenolpyruvate carboxylase in malate-accumulating sink tissues. *J.*
717 *Exp. Bot.* **68**, 5857–5869 (2017).

718 32. Blonde, J. D. & Plaxton, W. C. Structural and kinetic properties of high and low molecular
719 mass phosphoenolpyruvate carboxylase isoforms from the endosperm of developing castor
720 oilseeds. *J. Biol. Chem.* **278**, 11867–11873 (2003).

721 33. Michael, T. P. *et al.* Network discovery pipeline elucidates conserved time-of-day–specific
722 cis-regulatory modules. *PLoS Genet.* **4**, e14 (2008).

723 34. Filichkin, S. A. *et al.* Global profiling of rice and poplar transcriptomes highlights key
724 conserved circadian-controlled pathways and cis-regulatory modules. *PLoS One* **6**, e16907
725 (2011).

726 35. Michael, T. P. *et al.* Genome and time-of-day transcriptome of *Wolffia australiana* link
727 morphological minimization with gene loss and less growth control. *Genome Res.* **31**, 225–
728 238 (2020).

729 36. Ferrari, C. *et al.* Kingdom-wide comparison reveals the evolution of diurnal gene expression
730 in Archaeplastida. *Nat. Commun.* **10**, 1–13 (2019).

731 37. Steed, G., Ramirez, D. C., Hannah, M. A. & Webb, A. A. R. Chronoculture, harnessing the
732 circadian clock to improve crop yield and sustainability. *Science* **372**, (2021).

733 38. Corellou, F. *et al.* Clocks in the green lineage: comparative functional analysis of the
734 circadian architecture of the picoeukaryote *Ostreococcus*. *Plant Cell* **21**, 3436–3449 (2009).

735 39. Holm, K., Källman, T., Gyllenstrand, N., Hedman, H. & Lagercrantz, U. Does the core
736 circadian clock in the moss *Physcomitrella patens* (Bryophyta) comprise a single loop?
737 *BMC Plant Biol.* **10**, 1–14 (2010).

738 40. Kuo, L.-Y., Huang, Y.-J., Chang, J., Chiou, W.-L. & Huang, Y.-M. Evaluating the spore
739 genome sizes of ferns and lycophytes: a flow cytometry approach. *New Phytol.* **213**, 1974–
740 1983 (2017).

741 41. Ebihara, A. *et al.* Nuclear DNA, chloroplast DNA, and ploidy analysis clarified biological
742 complexity of the *Vandenboschia radicans* complex (Hymenophyllaceae) in Japan and
743 adjacent areas. *Am. J. Bot.* **92**, 1535–1547 (2005).

744 42. Praça-Fontes, M. M., Carvalho, C. R., Clarindo, W. R. & Cruz, C. D. Revisiting the DNA C-
745 values of the genome size-standards used in plant flow cytometry to choose the ‘best
746 primary standards’. *Plant Cell Rep.* **30**, 1183–1191 (2011).

747 43. Marçais, G. & Kingsford, C. A fast, lock-free approach for efficient parallel counting of
748 occurrences of k-mers. *Bioinformatics* **27**, 764–770 (2011).

749 44. Vulture, G. W. *et al.* GenomeScope: fast reference-free genome profiling from short reads.
750 *Bioinformatics* **33**, 2202–2204 (2017).

751 45. Kuo, L. Y. Polyploidy and biogeography in genus *Deparia* and phylogeography in *Deparia*
752 *lancea*. *PhD Thesis* (2015).

753 46. Li, H. Minimap and miniasm: fast mapping and de novo assembly for noisy long sequences.
754 *Bioinformatics* **32**, 2103–2110 (2016).

755 47. Vaser, R., Sović, I., Nagarajan, N. & Šikić, M. Fast and accurate de novo genome assembly
756 from long uncorrected reads. *Genome Res.* **27**, 737–746 (2017).

757 48. Walker, B. J. *et al.* Pilon: an integrated tool for comprehensive microbial variant detection
758 and genome assembly improvement. *PLoS One* **9**, e112963 (2014).

759 49. Laetsch, D. R. & Blaxter, M. L. BlobTools: Interrogation of genome assemblies. *F1000Res.*
760 **6**, 1287 (2017).

761 50. Xu, G.-C. *et al.* LR_Gapcloser: a tiling path-based gap closer that uses long reads to
762 complete genome assembly. *Gigascience* **8**, (2019).

763 51. Roach, M. J., Schmidt, S. A. & Borneman, A. R. Purge Haplontigs: allelic contig
764 reassignment for third-gen diploid genome assemblies. *BMC Bioinformatics* **19**, 460 (2018).

765 52. Jin, J.-J. *et al.* GetOrganelle: a fast and versatile toolkit for accurate de novo assembly of
766 organelle genomes. *Genome Biol.* **21**, 1–31 (2020).

767 53. Ou, S. & Jiang, N. LTR_retriever: A Highly Accurate and Sensitive Program for
768 Identification of Long Terminal Repeat Retrotransposons. *Plant Physiol.* **176**, 1410–1422
769 (2018).

770 54. Smit, A. F. A. & Hubley, R. *RepeatModeler Open-1.0*. Available online at
771 <http://www.repeatmasker.org>.

772 55. Smit, A. F. A., Hubley, R. & Green, P. *RepeatMasker Open-4.0*. Available online at:
773 <http://www.repeatmasker.org>.

774 56. Stanke, M. & Morgenstern, B. AUGUSTUS: a web server for gene prediction in eukaryotes
775 that allows user-defined constraints. *Nucleic Acids Res.* **33**, W465–W467 (2005).

776 57. Korf, I. Gene finding in novel genomes. *BMC Bioinformatics* **5**, 59 (2004).

777 58. Brůna, T., Hoff, K. J., Lomsadze, A., Stanke, M. & Borodovsky, M. BRAKER2: automatic
778 eukaryotic genome annotation with GeneMark-EP+ and AUGUSTUS supported by a
779 protein database. *NAR Genom Bioinform* **3**, lqaa108 (2021).

780 59. Grabherr, M. G. *et al.* Full-length transcriptome assembly from RNA-Seq data without a
781 reference genome. *Nat. Biotechnol.* **29**, 644–652 (2011).

782 60. Holt, C. & Yandell, M. MAKER2: an annotation pipeline and genome-database
783 management tool for second-generation genome projects. *BMC Bioinformatics* **12**, 491
784 (2011).

785 61. Huerta-Cepas, J. *et al.* Fast Genome-Wide Functional Annotation through Orthology
786 Assignment by eggNOG-Mapper. *Mol. Biol. Evol.* **34**, 2115–2122 (2017).

787 62. Pertea, M. *et al.* StringTie enables improved reconstruction of a transcriptome from RNA-
788 seq reads. *Nat. Biotechnol.* **33**, 290–295 (2015).

789 63. Amborella Genome Project. The *Amborella* genome and the evolution of flowering plants.
790 *Science* **342**, 1241089 (2013).

791 64. Lamesch, P. *et al.* The *Arabidopsis* Information Resource (TAIR): improved gene
792 annotation and new tools. *Nucleic Acids Res.* **40**, D1202–10 (2012).

793 65. International Brachypodium Initiative. Genome sequencing and analysis of the model grass
794 *Brachypodium distachyon*. *Nature* **463**, 763–768 (2010).

795 66. Yang, Y. *et al.* Prickly waterlily and rigid hornwort genomes shed light on early angiosperm
796 evolution. *Nat Plants* **6**, 215–222 (2020).

797 67. Tang, H. *et al.* An improved genome release (version Mt4.0) for the model legume
798 *Medicago truncatula*. *BMC Genomics* **15**, 312 (2014).

799 68. Ming, R. *et al.* Genome of the long-living sacred lotus (*Nelumbo nucifera* Gaertn.). *Genome*

800 *Biol.* **14**, R41 (2013).

801 69. Zhang, L. *et al.* The water lily genome and the early evolution of flowering plants. *Nature* **577**, 79–84 (2020).

802 70. Nystedt, B. *et al.* The Norway spruce genome sequence and conifer genome evolution. *Nature* **497**, 579–584 (2013).

803 71. Wang, W. *et al.* The *Spirodela polyrhiza* genome reveals insights into its neotenous reduction fast growth and aquatic lifestyle. *Nat. Commun.* **5**, 3311 (2014).

804 72. Ibarra-Laclette, E. *et al.* Architecture and evolution of a minute plant genome. *Nature* **498**, 94–98 (2013).

805 73. Jaillon, O. *et al.* The grapevine genome sequence suggests ancestral hexaploidization in major angiosperm phyla. *Nature* **449**, 463–467 (2007).

806 74. Olsen, J. L. *et al.* The genome of the seagrass *Zostera marina* reveals angiosperm adaptation to the sea. *Nature* **530**, 331–335 (2016).

807 75. Cheng, S. *et al.* Genomes of Subaerial Zygematophyceae Provide Insights into Land Plant Evolution. *Cell* **179**, 1057–1067.e14 (2019).

808 76. Conway, J. R., Lex, A. & Gehlenborg, N. UpSetR: an R package for the visualization of intersecting sets and their properties. *Bioinformatics* **33**, 2938–2940 (2017).

809 77. Kim, D., Paggi, J. M., Park, C., Bennett, C. & Salzberg, S. L. Graph-based genome alignment and genotyping with HISAT2 and HISAT-genotype. *Nat. Biotechnol.* **37**, 907–915 (2019).

810 78. Li, H. *et al.* The Sequence Alignment/Map format and SAMtools. *Bioinformatics* **25**, 2078–2079 (2009).

811 79. Li, H. A statistical framework for SNP calling, mutation discovery, association mapping and population genetical parameter estimation from sequencing data. *Bioinformatics* **27**, 2987–2993 (2011).

812 80. Quinlan, A. R. & Hall, I. M. BEDTools: a flexible suite of utilities for comparing genomic features. *Bioinformatics* **26**, 841–842 (2010).

813 81. Zwaenepoel, A. & Van de Peer, Y. wgd—simple command line tools for the analysis of ancient whole-genome duplications. *Bioinformatics* **35**, 2153–2155 (2019).

814 82. Xie, Y. *et al.* SOAPdenovo-Trans: de novo transcriptome assembly with short RNA-Seq reads. *Bioinformatics* **30**, 1660–1666 (2014).

815 83. Barker, M. S. *et al.* Multiple paleopolyploidizations during the evolution of the Compositae reveal parallel patterns of duplicate gene retention after millions of years. *Mol. Biol. Evol.* **25**, 2445–2455 (2008).

816 84. Barker, M. S. *et al.* EvoPipes.net: Bioinformatic Tools for Ecological and Evolutionary Genomics. *Evol. Bioinform. Online* **6**, 143–149 (2010).

817 85. Birney, E., Clamp, M. & Durbin, R. GeneWise and Genomewise. *Genome Res.* **14**, 988–995 (2004).

818 86. Goodstein, D. M. *et al.* Phytozome: a comparative platform for green plant genomics. *Nucleic Acids Res.* **40**, D1178–86 (2012).

819 87. Yang, Z. PAML 4: phylogenetic analysis by maximum likelihood. *Mol. Biol. Evol.* **24**, 1586–1591 (2007).

820 88. Benaglia, T., Chauveau, D., Hunter, D. & Young, D. Mixtools: An R package for analyzing finite mixture models. *J. Stat. Softw.* **32**, 1–29 (2009).

821 89. Loyer, A. & Goldman, N. Phylogeny-aware gap placement prevents errors in sequence alignment and evolutionary analysis. *Science* **320**, 1632–1635 (2008).

822 90. Ronquist, F. *et al.* MrBayes 3.2: efficient Bayesian phylogenetic inference and model choice across a large model space. *Syst. Biol.* **61**, 539–542 (2012).

823 91. Szöllősi, G.J. *et al.* Lateral gene transfer from the dead. *Syst. Biol.* **62**, 386–397 (2013).

824 92. Paradis, E. & Schliep, K. ape 5.0: an environment for modern phylogenetics and evolutionary analyses in R. *Bioinformatics* **35**, 526–528 (2019).

851 93. Morris, J. L. *et al.* The timescale of early land plant evolution. *Proc. Natl. Acad. Sci. U. S. A.*
852 **115**, E2274–E2283 (2018).

853 94. Larsén, E. & Rydin, C. Disentangling the phylogeny of *Isoetes* (Isoetales), using nuclear
854 and plastid data. *Int. J. Plant Sci.* **177**, 157–174 (2016).

855 95. Edgar, R. C. MUSCLE: multiple sequence alignment with high accuracy and high
856 throughput. *Nucleic Acids Res.* **32**, 1792–1797 (2004).

857 96. Kalyaanamoorthy, S., Minh, B. Q., Wong, T. K. F., von Haeseler, A. & Jermiin, L. S.
858 ModelFinder: fast model selection for accurate phylogenetic estimates. *Nat. Methods* **14**,
859 587–589 (2017).

860 97. Nguyen, L.-T., Schmidt, H. A., von Haeseler, A. & Minh, B. Q. IQ-TREE: a fast and effective
861 stochastic algorithm for estimating maximum-likelihood phylogenies. *Mol. Biol. Evol.* **32**,
862 268–274 (2015).

863 98. Hoang, D. T., Chernomor, O., von Haeseler, A., Minh, B. Q. & Vinh, L. S. UFBoot2:
864 Improving the Ultrafast Bootstrap Approximation. *Mol. Biol. Evol.* **35**, 518–522 (2018).

865 99. de Vries, S. *et al.* The evolution of the phenylpropanoid pathway entailed pronounced
866 radiations and divergences of enzyme families. *bioRxiv* 2021.05.27.445924 (2021)
867 doi:10.1101/2021.05.27.445924.

868 100. Slotte, T. *et al.* The *Capsella rubella* genome and the genomic consequences of rapid
869 mating system evolution. *Nat. Genet.* **45**, 831–835 (2013).

870 101. Wan, T. *et al.* A genome for gnetophytes and early evolution of seed plants. *Nat. Plants* **4**,
871 82–89 (2018).

872 102. Sierro, N. *et al.* The tobacco genome sequence and its comparison with those of tomato
873 and potato. *Nat. Commun.* **5**, 1–9 (2014).

874 103. Ouyang, S. *et al.* The TIGR Rice Genome Annotation Resource: improvements and new
875 features. *Nucleic Acids Res.* **35**, D883–7 (2007).

876 104. Argout, X. *et al.* The genome of *Theobroma cacao*. *Nat. Genet.* **43**, 101–108 (2011).

877 105. Wang, S. *et al.* Genomes of early-diverging streptophyte algae shed light on plant
878 terrestrialization. *Nat. Plants* **6**, 95–106 (2020).

879 106. Nishiyama, T. *et al.* The *Chara* genome: secondary complexity and implications for plant
880 terrestrialization. *Cell* **174**, 448–464.e24 (2018).

881 107. Hori, K. *et al.* *Klebsormidium flaccidum* genome reveals primary factors for plant terrestrial
882 adaptation. *Nat. Commun.* **5**, 3978 (2014).

883 108. Jiao, C. *et al.* The *Penium margaritaceum* genome: hallmarks of the origins of land plants.
884 *Cell* **181**, 1097–1111.e12 (2020).

885 109. de Vries, J. *et al.* Heat stress response in the closest algal relatives of land plants reveals
886 conserved stress signaling circuits. *Plant J.* **103**, 1025–1048 (2020).

887 110. de Vries, J., Curtis, B. A., Gould, S. B. & Archibald, J. M. Embryophyte stress signaling
888 evolved in the algal progenitors of land plants. *Proc. Natl. Acad. Sci. U. S. A.* **115**, E3471–
889 E3480 (2018).

890 111. Ju, C. *et al.* Conservation of ethylene as a plant hormone over 450 million years of
891 evolution. *Nat. Plants* **1**, 14004 (2015).

892 112. Moreau, H. *et al.* Gene functionalities and genome structure in *Bathycoccus prasinos* reflect
893 cellular specializations at the base of the green lineage. *Genome Biol.* **13**, R74 (2012).

894 113. Merchant, S. S. *et al.* The *Chlamydomonas* genome reveals the evolution of key animal
895 and plant functions. *Science* **318**, 245–250 (2007).

896 114. Blanc, G. *et al.* The genome of the polar eukaryotic microalga *Coccomyxa subellipsoidea*
897 reveals traits of cold adaptation. *Genome Biol.* **13**, R39 (2012).

898 115. Worden, A. Z. *et al.* Green evolution and dynamic adaptations revealed by genomes of the
899 marine picoeukaryotes *Micromonas*. *Science* **324**, 268–272 (2009).

900 116. Palenik, B. *et al.* The tiny eukaryote *Ostreococcus* provides genomic insights into the
901 paradox of plankton speciation. *Proc. Natl. Acad. Sci. U. S. A.* **104**, 7705–7710 (2007).

902 117. De Clerck, O. *et al.* Insights into the evolution of multicellularity from the sea lettuce
903 genome. *Curr. Biol.* **28**, 2921–2933.e5 (2018).

904 118. Prochnik, S. E. *et al.* Genomic analysis of organismal complexity in the multicellular green
905 alga *Volvox carteri*. *Science* **329**, 223–226 (2010).

906 119. de Vries, J., de Vries, S., Slamovits, C. H., Rose, L. E. & Archibald, J. M. How
907 embryophytic is the biosynthesis of phenylpropanoids and their derivatives in Streptophyte
908 algae? *Plant Cell Physiol.* **58**, 934–945 (2017).

909 120. Katoh, K. & Standley, D. M. MAFFT multiple sequence alignment software version 7:
910 improvements in performance and usability. *Mol. Biol. Evol.* **30**, 772–780 (2013).

911 121. Minh, B. Q. *et al.* IQ-TREE 2: New models and efficient methods for phylogenetic inference
912 in the genomic Era. *Mol. Biol. Evol.* **37**, 1530–1534 (2020).

913 122. Hu, Y. *et al.* Crystal structures of a *Populus tomentosa* 4-coumarate:CoA ligase shed light
914 on its enzymatic mechanisms. *Plant Cell* **22**, 3093–3104 (2010).

915 123. Pan, H. *et al.* Structural studies of cinnamoyl-CoA reductase and cinnamyl-alcohol
916 dehydrogenase, key enzymes of monolignol biosynthesis. *Plant Cell* **26**, 3709–3727 (2014).

917 124. Louie, G. V. *et al.* Structure-function analyses of a caffeic acid O-methyltransferase from
918 perennial ryegrass reveal the molecular basis for substrate preference. *Plant Cell* **22**,
919 4114–4127 (2010).

920 125. Youn, B. *et al.* Crystal structures and catalytic mechanism of the *Arabidopsis* cinnamyl
921 alcohol dehydrogenases AtCAD5 and AtCAD4. *Org. Biomol. Chem.* **4**, 1687–1697 (2006).

922 126. Ferrer, J.-L., Zubietta, C., Dixon, R. A. & Noel, J. P. Crystal structures of alfalfa caffeoyl
923 coenzyme A 3-O-methyltransferase. *Plant Physiol.* **137**, 1009–1017 (2005).

924 127. Barbier, F. F. *et al.* A phenol/chloroform-free method to extract nucleic acids from
925 recalcitrant, woody tropical species for gene expression and sequencing. *Plant Methods* **15**,
926 62 (2019).

927 128. Love, M., Anders, S. & Huber, W. Differential analysis of count data--the DESeq2 package.
928 *Genome Biol.* **15**, 10–1186 (2014).

929 129. Conesa, A., Nueda, M. J., Ferrer, A. & Talón, M. maSigPro: a method to identify
930 significantly differential expression profiles in time-course microarray experiments.
931 *Bioinformatics* **22**, 1096–1102 (2006).

932 130. MacKinnon, Kirk J-M., et al. Changes in ambient temperature are the prevailing cue in
933 determining *Brachypodium distachyon* diurnal gene regulation. *New Phytologist* **227**, 1709–
934 1724 (2020).

935 131. Michael, T. P. *et al.* A morning-specific phytohormone gene expression program underlying
936 rhythmic plant growth. *PLoS Biol.* **6**, e225 (2008).

937 132. Mockler, T. C. *et al.* The DIURNAL project: DIURNAL and circadian expression profiling,
938 model-based pattern matching, and promoter analysis. *Cold Spring Harb. Symp. Quant.
939 Biol.* **72**, 353–363 (2007).

940 133. McLeay, R. C. & Bailey, T. L. Motif Enrichment Analysis: a unified framework and an
941 evaluation on ChIP data. *BMC Bioinformatics* **11**, 165 (2010).

942 134. Franco-Zorrilla, J. M. *et al.* DNA-binding specificities of plant transcription factors and their
943 potential to define target genes. *Proc. Natl. Acad. Sci. U. S. A.* **111**, 2367–2372 (2014).

944 135. Grant, C. E., Bailey, T. L. & Noble, W. S. FIMO: scanning for occurrences of a given motif.
945 *Bioinformatics* **27**, 1017–1018 (2011).

946

947

948

949

950

951 **Acknowledgements:**

952 The authors would like to thank Karolina Heyduk, Peter Schafran, and Arthur Zwaenepoel for
953 their advice and support to various aspects of this project. J.d.V. is supported through funding
954 from the European Research Council (ERC) under the European Union's Horizon 2020
955 research and innovation programme (grant no. 852725; ERC Starting Grant 'TerreStriAL').
956 A.D.A. and A.D. are grateful for being supported through the International Max Planck Research
957 School (IMPRS) for Genome Science.

958

959 **Author contributions:**

960 D.W., L.-Y.K., T.P.M. and F.-W.L. coordinated the project. Y.-M.H. provided the plant materials.
961 L.-Y.K. carried out the time-course experiment and nucleic acid extraction. T.P.M. and F.-W.L.
962 sequenced and assembled the genome. H.-P.Y. and F.-W.L. annotated the genome. D.W.
963 assembled the plastome and profiled RNA-editing. D.W. circumscribed gene families and
964 examined genes related to stomata and root development. A.D.A., I.I., A.M., S.d.V. and J.d.V.
965 characterized lignin biosynthesis genes. D.W., Z.L. and M.S.B. carried out WGD analysis. D.W.
966 analyzed expressions of CAM pathway genes. N.T.H. and T.P.M. carried out HAYSTACK and
967 ELEMENT analyses. D.W., T.P.M. and F.-W.L. synthesized and wrote the manuscript.

968

969 **Competing interests:**

970 The authors declare no competing interests.